Sub-40 fs, 1060-nm Yb-fiber laser enhances penetration depth in nonlinear optical microscopy of human skin

Mihaela Balu,[a,*,†] Ilyas Saytashev,[b,†] Jue Hou,[a] Marcos Dantus,[b] and Bruce J. Tromberg[a]
[a]University of California, Irvine, Beckman Laser Institute, Laser Microbeam and Medical Program, 1002 Health Sciences Road, Irvine, California 92612, United States
[b]Michigan State University, Department of Chemistry, 578 South Shaw Lane, East Lansing, Michigan 48824, United States

Abstract. Advancing the practical utility of nonlinear optical microscopy requires continued improvement in imaging depth and contrast. We evaluated second-harmonic generation (SHG) and third-harmonic generation images from *ex vivo* human skin and showed that a sub-40 fs, 1060-nm Yb-fiber laser can enhance SHG penetration depth by up to 80% compared to a >100 fs, 800 nm Ti:sapphire source. These results demonstrate the potential of fiber-based laser systems to address a key performance limitation related to nonlinear optical microscopy (NLOM) technology while providing a low-barrier-to-access alternative to Ti:sapphire sources that could help accelerate the movement of NLOM into clinical practice. [DOI: 10.1117/1.JBO.20.12.120501]

Keywords: nonlinear optical microscopy human skin; third-harmonic generation microscopy; multiphoton microscopy; multimodal microscopy; optical biopsy; depth resolved imaging; Yb-fiber laser; adaptive phase-amplitude pulse shaper.

Paper 150438LRR received Jun. 29, 2015; accepted for publication Oct. 30, 2015; published online Dec. 7, 2015.

In vivo, label-free nonlinear optical microscopy (NLOM) of human skin is under investigation for a broad range of clinical applications spanning from skin cancer detection and diagnosis[1–4] to characterizing and understanding keratinocyte metabolism,[5] skin aging,[6,7] pigment biology,[8,9] and cosmetic treatments.[10–12] NLOM signals are derived from several sources including cellular cofactors, melanin, and extracellular matrix proteins. Although exceptionally rich in both anatomic and functional contrast, NLOM has relatively limited penetration depth in turbid materials. This is due to the fact that multiple light scattering diminishes the instantaneous excitation intensity and nonlinear signal generation in the focused laser beam. As a result, there is considerable interest in exploring how light source performance can be optimized to improve imaging depth. Ti:sapphire lasers, commonly used in NLOM imaging, are generally able to access the superficial dermis of human skin to depths of 150 to 200 μm. Penetration depth primarily depends on the material scattering length at the excitation wavelength, the efficiency of the nonlinear excitation process, the excitation average power, repetition rate, pulse width, and the detection geometry.[13,14] Adjusting these parameters in order to improve the penetration depth has been explored in several studies using Ti:sapphire and optical parametric oscillator-based femtosecond lasers as excitation light sources.[15–21] Sun et al. have shown that reduced light scattering using a Cr:Forsterite 1230 to 1250 nm source can increase penetration depth up to 300 μm for harmonic generation imaging of human skin.[22] Improvements in penetration depth can also be achieved when using shorter laser pulse widths.[16] Depth resolved imaging studies require higher average laser powers and thermal damage to tissue becomes an issue of concern.[23,24] Photothermal absorption of tissue is wavelength dependent, and so is the damage threshold. Heating following laser exposure at 800 nm is five times greater than at 1060 nm, and the damage threshold at 800 nm is three times lower than at 1060 nm.[25] With the development of next-generation fiber lasers, it is possible to imagine combining these technical features with more compact, portable, and inexpensive light sources that could facilitate clinical translation of NLOM technology.

Fiber-based laser sources have been used for NLOM imaging of thin tissue cross-sections,[26–28] mouse brain,[29] and human skin tissue[30] using fluorescence labeling. In this work, we evaluate the performance of a sub-40 fs, 1060-nm Yb-fiber laser for label-free NLOM imaging of human skin. The effect of excitation wavelength and pulse width on penetration depth in thick, turbid tissues is determined by comparing the fiber laser to an 800 nm Ti:sapphire laser source. We employ the depth-dependent decay of second-harmonic generation (SHG) signals as a standard metric for evaluating performance.

The excitation laser sources used were a Ti:sapphire oscillator (MIRA 900; Coherent Inc.; 220 fs, 76 MHz, 600 mW output power, tuning wavelength 720 to 980 nm) tuned to 800 nm for this study and a Yb-fiber laser (BioPhotonic Solutions Inc., 1060 nm, sub-40 fs, 39.2 MHz, 200 mW compressed output power). The prototype Yb-fiber laser, with self-similar pulse evolution,[28] has an integrated adaptive phase-amplitude pulse shaper (MIIPS-HD, BioPhotonic Solutions Inc.) based on a 4f configuration with a two-dimensional spatial light modulator. The purpose of the pulse shaper was to control high-order phase distortions introduced by the high numerical-aperture (NA) objective and other dispersive elements in the beam path. The 1060-nm pulses were compressed to nearly transform limited duration using multiphoton intrapulse interference phase scan (MIIPS),[31] and their full-width half maximum duration was measured by interferometric autocorrelation using the microscope detection unit (BioPhotonic Solutions Inc.) at the focal plane. Each of the two excitation beams (800 and 1060 nm) was directed toward our home-built laser-scanning microscope and focused into the sample by an Olympus objective (XLPL25XWMP, 25× /1.05 NA water). The nonlinear signals from the sample were epi-collected and directed toward two photomultiplier tubes (R3896, Hamamatsu) by a dichroic

*Address all correspondence to: Mihaela Balu, E-mail: mihaela.b@uci.edu

†Authors contributed equally.

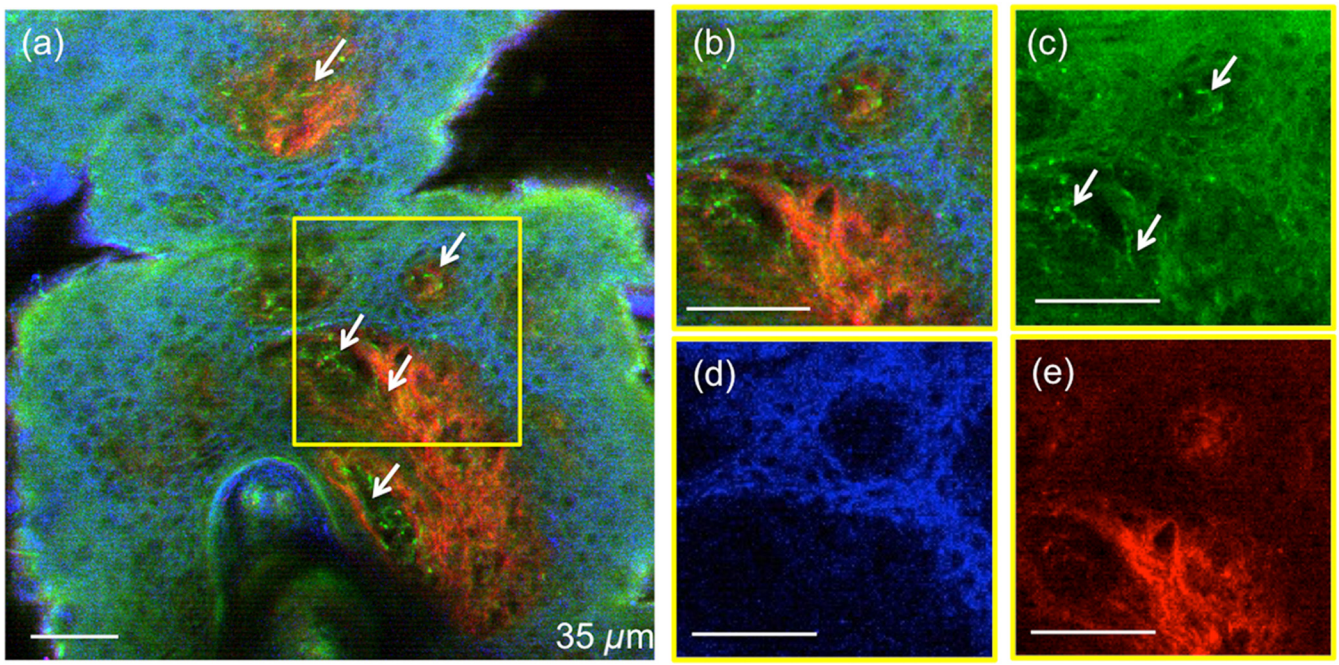

Fig. 1 Multimodal nonlinear optical microscopy (NLOM) images of human skin acquired with 800- and 1060-nm excitation wavelengths at the same depth. (a) Epidermal-dermal junction in human skin imaged by third-harmonic generation (THG) (blue) and second-harmonic generation (SHG) (red) using 1060 nm and by two-photon excited fluorescence (TPEF) (green) using 800 nm as excitation wavelengths ($z = 35$ μm). TPEF signal originates from keratin in the epidermal keratinocytes and from elastin fibers (arrows) in the superficial papillary dermis, while THG signal highlights the keratinocytes only; SHG signal originates from collagen fibers. (b) Multimodal NLOM image corresponding to the inset in (a) representing contribution from three channels: (c) TPEF signal from keratinocytes and elastin fibers (arrows), (d) THG signal from keratinocytes, and (e) SHG signal from collagen fibers. Scale bar is 50 μm.

mirror (Semrock, Inc., 510 LP). The dichroic mirror was used to split the emission signal into two spectral channels defined by the emission filters: 440 SP; 375/110 BP and 720 SP; 535/150 BP (Semrock Inc.). We used discarded human skin tissue (fixed in formalin) to test the effect of sub-40 fs, 1060-nm excitation laser pulses on depth penetration in this sample. For each excitation wavelength (800 and 1060 nm), we acquired five stacks of images as optical sections of $\sim 430 \times 430$ μm^2 (512×512 pixels) at different depths ranging from 0 to 200 μm (2 μm step). In the sample studied in this work, the main contrast mechanisms for 800-nm excitation are based on two-photon excited fluorescence (TPEF) signals from keratin, melanin, and elastin fibers and on SHG signals from collagen fibers. When using 1060 nm as excitation, the epidermis is visualized by third-harmonic generation (THG) contrast derived from refractive index discontinuities at interfaces, while dermal contrast is derived from collagen fiber SHG.

Figure 1 shows merged images of human skin acquired at the same depth with 800- and 1060-nm excitation. THG imaging of the keratinocyte structure in human skin epidermis using 1230 nm as excitation has been reported by Sun et al. in several studies.[6,22] THG is not generated by elastin fibers in human dermis, although signals from elastic cartilage have been observed.[32]

Figure 2 shows representative images corresponding to one of the stacks acquired in the same location of the sample by using 800 and 1060 nm as excitation. The images in Figs. 2(a)–2(c) and 2(f)–2(h) represent en-face (x-y plane) images acquired at different depths. The cross-sectional (x-z plane) images shown in Figs. 2(d) and 2(e) were obtained from three-dimensional (3-D) image reconstruction of en-face stacks using Amira (FEI Inc.).

To compare the penetration depth attained by each excitation wavelength, we adjusted the laser powers (40 mW for 800 nm and 20 mW for 1060 nm) such that the average intensity of the SHG signal corresponding to the sample surface ($z = 0$) was similar for both wavelengths. The laser power and all the other experimental parameters were kept the same during the data acquisition. The SHG signals measured in the dermis of the skin sample are plotted versus depth in Fig. 2 on log scale. The signal calculated at each depth represents the average of the pixel intensities in the SHG images at that particular depth. The SHG intensity decay curve was normalized to the maximum intensity value for each wavelength.

The SHG intensity decays as a function of depth z according $I_{\mathrm{SHG}} \sim \exp(-Az)$, where A is the attenuation coefficient that includes the sample absorption and scattering properties at both the excitation and emission wavelengths. The inverse of A yields a $1/e$ attenuation length of 49 μm for 800 nm and 88 μm for 1060 nm, an increase of $\sim$80% for the Yb-fiber laser source. Similar results were obtained for all five stacks acquired in the sample, which shows that 1060 nm, sub-40 fs pulses can provide deeper penetration in highly scattering samples, such as skin.

In summary, these results demonstrate the potential of fiber-based laser systems to be used as excitation light sources for NLOM imaging of highly turbid media. Despite their current lack of tunability, short-pulse, >1 μm wavelength fiber lasers can provide a low-barrier-to-access alternative to conventional Ti:sapphire lasers. They are of particular interest in applications

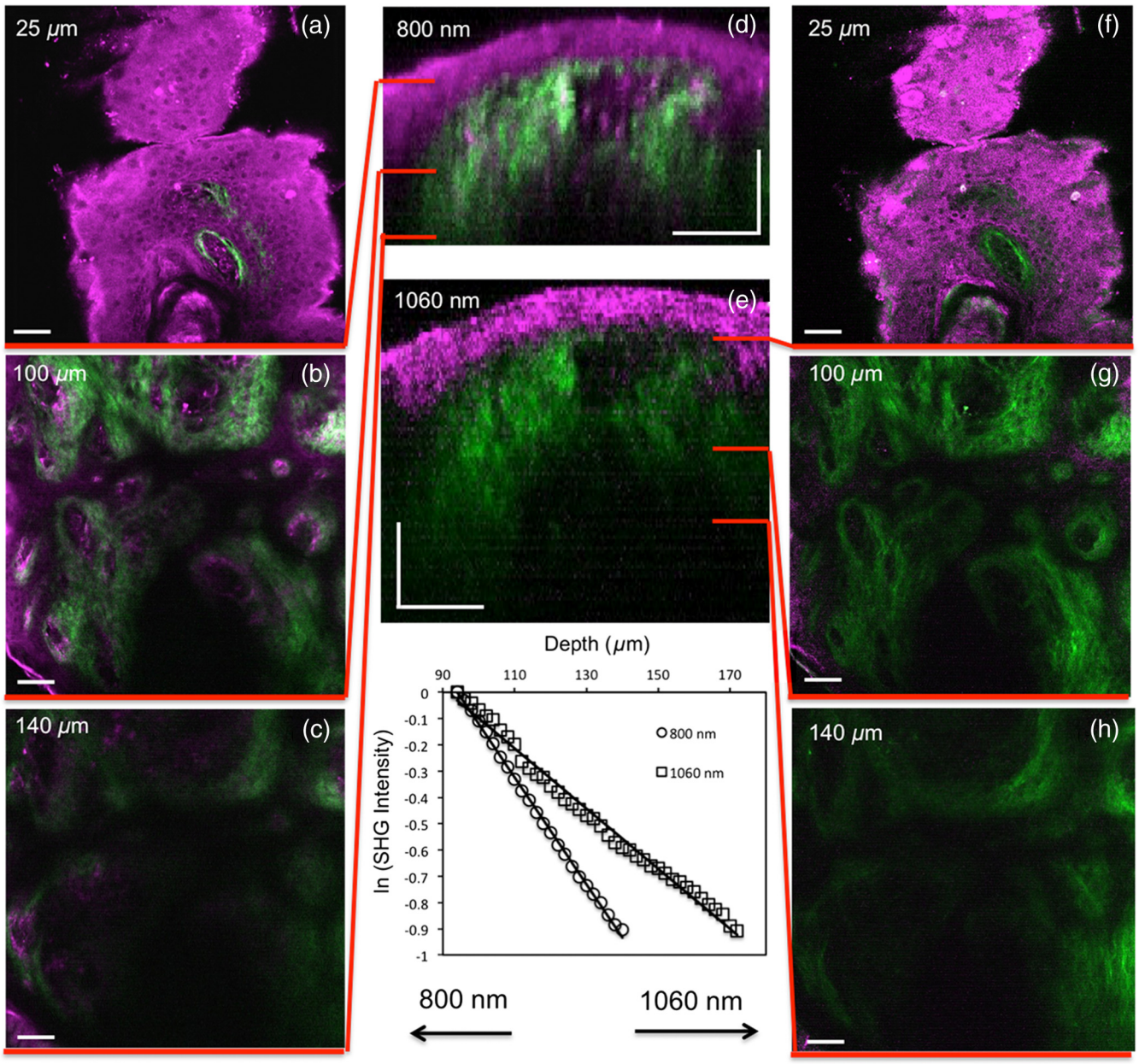

Fig. 2 *Ex vivo* imaging of human skin using 800 nm (Ti:sapphire laser) and 1060 nm (Yb-fiber laser). (a–c) Horizontal sections (*x*-*y* scans) at different depths corresponding to 800-nm excitation wavelength. The optical sections show images of the epidermal cells through the TPEF signal (magenta, $z = 25$ μm); collagen fibers (green; SHG signal) and elastin fibers (magenta, TPEF signal) ($z = 100$ μm; 140 μm). Vertical sections were obtained from three-dimensional reconstruction for (d) 800-nm and (e) 1060-nm excitation wavelengths (40 mW for 800 nm and 20 mW for 1060 nm). Horizontal sections (*x*-*y* scans) at different depths corresponding to 800- and 1060-nm excitation wavelengths are shown in (a–c), (f–h), respectively. The optical sections show images of the epidermal cells through the THG signal (magenta, $z = 25$ μm) and collagen fibers (green; SHG signal) ($z = 100$ μm; 140 μm). Scale bar is 50 μm. The plot represents the SHG signal attenuation (logarithmic scale) with depth, for 800- and 1060-nm excitation wavelengths.

related to *in vivo* imaging of human skin as they can deliver up to 80% improvement in SHG imaging depth compared to conventionally used Ti:sapphire lasers. An additional benefit for *in vivo* human skin imaging is related to the THG contrast mechanism which, unlike TPEF, does not involve absorption and might allow for the use of higher excitation powers. With continued development of expanded wavelengths, powers, and pulse characteristics, these systems are expected to increase in use, particularly in skin studies where assessment of 3-D morphology is important.

Acknowledgments

We would like to thank BioPhotonic Solutions Inc. for making their laser prototype available for these measurements and, in particular, Dr. Bingwei Xu for installing the laser system at UC Irvine. This research was supported partially by the

National Institutes of Health (NIH) NIBIB Laser Microbeam and Medical Program (LAMMP, P41-EB015890), Air Force Research Laboratory Agreement No. FA9550-04-1-0101, and the Arnold and Mabel Beckman Foundation.

References

1. M. Balu et al., "Distinguishing between benign and malignant melanocytic nevi by in vivo multiphoton microscopy," *Cancer Res.* **74**(10), 2688–2697 (2014).
2. M. Balu et al., "In vivo multiphoton microscopy of basal cell carcinoma," *JAMA Dermatol.* **151**(10), 1068–1074 (2015).
3. E. Dimitrow et al., "Sensitivity and specificity of multiphoton laser tomography for in vivo and ex vivo diagnosis of malignant melanoma," *J. Invest. Dermatol.* **129**(7), 1752–1758 (2009).
4. M. Ulrich et al., "In vivo detection of basal cell carcinoma: comparison of a reflectance confocal microscope and a multiphoton tomography," *J. Biomed. Opt.* **18**(6), 061229 (2013).
5. M. Balu et al., "In vivo multiphoton NADH fluorescence reveals depth-dependent keratinocyte metabolism in human skin," *Biophys. J.* **104**(1), 258–267 (2013).
6. Y. H. Liao et al., "Quantitative analysis of intrinsic skin aging in dermal papillae by in vivo harmonic generation microscopy," *Biomed. Opt. Express* **5**(9), 3266–3279 (2014).
7. M. J. Koehler et al., "In vivo assessment of human skin aging by multiphoton laser scanning tomography," *Opt. Lett.* **31**(19), 2879–2881 (2006).
8. T. B. Krasieva et al., "Two-photon excited fluorescence lifetime imaging and spectroscopy of melanins in vitro and in vivo," *J. Biomed. Opt.* **18**(3), 031107 (2013).
9. Y. Dancik et al., "Use of multiphoton tomography and fluorescence lifetime imaging to investigate skin pigmentation in vivo," *J. Biomed. Opt.* **18**(2), 026022 (2013).
10. R. Bazin et al., "Clinical study on the effects of a cosmetic product on dermal extracellular matrix components using a high-resolution multiphoton tomography," *Skin Res. Technol.* **16**(3), 305–310 (2010).
11. V. R. Leite-Silva et al., "The effect of formulation on the penetration of coated and uncoated zinc oxide nanoparticles into the viable epidermis of human skin in vivo," *Eur. J. Pharm. Biopharm.* **84**(2), 297–308 (2013).
12. J. Lademann et al., "In vivo methods for the analysis of the penetration of topically applied substances in and through the skin barrier," *Int. J. Cosmet. Sci.* **34**(6), 551–559 (2012).
13. M Oheim et al., "Two-photon microscopy in brain tissue: parameters influencing the imaging depth," *J. Neurosci. Methods* **111**(1), 29–37 (2001).
14. F. Helmchen and W. Denk, "Deep tissue two-photon microscopy," *Nat. Methods* **2**(12), 932–940 (2005).
15. P. Theer, M. T. Hasan, and W. Denk, "Two-photon imaging to a depth of 1000 micron in living brains by use of a $Ti:Al_2O_3$ regenerative amplifier," *Opt. Lett.* **28**(12), 1022–1024 (2003).
16. S. Tang et al., "Effect of pulse duration on two-photon excited fluorescence and second harmonic generation in nonlinear optical microscopy," *J. Biomed. Opt.* **11**(2), 020501 (2006).
17. M. Balu et al., "Effect of excitation wavelength on penetration depth in nonlinear optical microscopy of turbid media," *J. Biomed. Opt.* **14**(1), 010508 (2009).
18. D. Kobat et al., "Deep tissue multiphoton microscopy using longer wavelength excitation," *Opt. Express* **17**(16), 13354–13364 (2009).
19. P. Xi et al., "Two-photon imaging using adaptive phase compensated ultrashort laser pulses," *J. Biomed. Opt.* **14**(1), 014002 (2009).
20. V. Andresen et al., "Infrared multiphoton microscopy: subcellular-resolved deep tissue imaging," *Curr. Opin. Biotechnol.* **20**(1), 54–62 (2009).
21. D. Kobat, N. G. Horton, and C. Xu, "In vivo two-photon microscopy to 1.6-mm depth in mouse cortex," *J. Biomed. Opt.* **16**(10), 106014 (2011).
22. S. Y. Chen, H. Y. Wu, and C. K. Sun, "In vivo harmonic generation biopsy of human skin," *J. Biomed. Opt.* **14**(6), 060505 (2009).
23. B. R. Masters et al., "Mitigating thermal mechanical damage potential during two-photon dermal imaging," *J. Biomed. Opt.* **9**(6), 1265–1270 (2004).
24. I. Saytashev et al., "Pulse duration and energy dependence of photodamage and lethality induced by femtosecond near infrared laser pulses in Drosophila melanogaster," *J. Photochem. Photobiol. B* **115**, 42–50 (2012).
25. J. N. Bixler et al., "Assessment of tissue heating under tunable near-infrared radiation," *J. Biomed. Opt.* **19**(7), 070501 (2014).
26. R. Galli et al., "Non-linear optical microscopy of kidney tumours," *J. Biophotonics* **7**(1–2), 23–27 (2014).
27. R. Galli et al., "Vibrational spectroscopic imaging and multiphoton microscopy of spinal cord injury," *Anal. Chem.* **84**(20), 8707–8714 (2012).
28. B. Nie et al., "Multimodal microscopy with sub-30 fs Yb fiber laser oscillator," *Biomed. Opt. Express* **3**(7), 1750–1756 (2012).
29. N. G. Horton et al., "In vivo three-photon microscopy of subcortical structures within an intact mouse brain," *Nat. Photonics* **7**(3), 205–209 (2013).
30. S. Tang et al., "Developing compact multiphoton systems using femtosecond fiber lasers," *J. Biomed. Opt.* **14**(3), 030508 (2009).
31. Y. Coello et al., "Interference without an interferometer: a different approach to measuring, compressing, and shaping ultrashort laser pulses," *J. Opt. Soc. Am. B* **25**(6), A140–A150 (2008).
32. C. H. Yu et al., "In vivo and ex vivo imaging of intra-tissue elastic fibers using third-harmonic-generation microscopy," *Opt. Express* **15**(18), 11167–11177 (2007).